

Symmetry-preserving WENO limiters

Xiaodong Liu, Nathaniel R. Morgan*, Donald E. Burton

X-Computational Physics Division; Los Alamos National Laboratory; P.O. Box 1663, Los Alamos, NM, USA

Abstract

Weighted essentially non-oscillatory (WENO) reconstruction schemes are presented that preserve cylindrical symmetry for radial flows on an equal-angle polar mesh. These new WENO schemes are used with a Lagrangian discontinuous Galerkin (DG) hydrodynamic method. The solution polynomials are reconstructed using the WENO schemes where the DG solution is the central stencil. A suite of challenging test problems are calculated to demonstrate the accuracy and robustness of the new WENO schemes.

Keywords: Lagrangian shock hydrodynamics, Discontinuous Galerkin, Cell-centered hydrodynamics, Symmetry-preserving WENO

1. Introduction

Lagrangian hydrodynamic methods, *e.g.*, staggered-grid hydrodynamics (SGH) [2, 3, 4, 5, 6] and cell-centered hydrodynamics (CCH)[7, 8, 9, 10, 11, 12, 13, 14], solve the governing equations for gas (or solid) dynamics on a mesh that moves and deforms with the flow. DG methods [15, 16, 17, 18] have been developed for Lagrangian hydrodynamics [19, 20, 21, 1, 22, 23, 24, 25]. For strong shock problems, both Barth-Jespersen limiter [26, 27] and the WENO reconstruction method [28, 29, 30, 31] have been explored with Lagrangian DG methods [20, 21, 23, 24, 25, 19]. However, the research on symmetry preserving WENO reconstruction schemes is quite limited [32], and as such, it is the focus of this paper.

In [1], the modal DG method generates a system of equations to evolve the coefficients for a Taylor series polynomial forward in time. The specific volume, velocity, and specific total energy fields are approximated with Taylor series polynomials about the mass center of a reference cell. The Lagrangian DG hydrodynamic method conserves mass, momentum, and total energy. An explicit TVD Runge-Kutta (RK) method is employed for time marching. In order to preserve cylindrical symmetry for radial flows on an equal-angle polar mesh, new WENO schemes are presented that build the WENO reconstruction by either projecting to a local orthonormal basis [33] or using a local characteristic decomposition [34]. These

*Corresponding author

Email addresses: xliu@lanl.gov (Xiaodong Liu), nmorgan@lanl.gov (Nathaniel R. Morgan), burton@lanl.gov (Donald E. Burton)

Preprint submitted to Elsevier

August 22, 2019

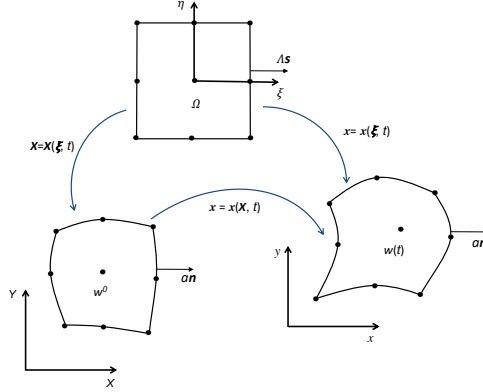


Figure 1: The map from the initial configuration ($X - Y$) and the map from a reference cell ($\xi - \eta$) are graphically illustrated. The cells will deform with the flow and the volume at a later time will be $w(t)$.

WENO schemes are used with a Lagrangian DG method in this work where the DG solution is used as a central stencil. These WENO schemes could also be used with finite volume CCH methods where the central stencil is constructed by least squares fitting neighboring cell average values.

2. Discretization

The differential Lagrangian equations for the specific volume (ν), velocity (\mathbf{u}), and specific total energy (τ) evolution are given by,

$$\rho \frac{d\nu}{dt} = \nabla \cdot \mathbf{u}, \quad \rho \frac{d\mathbf{u}}{dt} = \nabla \cdot \boldsymbol{\sigma}, \quad \rho \frac{d\tau}{dt} = \nabla \cdot (\boldsymbol{\sigma} \mathbf{u}), \quad (1)$$

where $\boldsymbol{\sigma}$ is the stress tensor. The pressure, specific internal energy and specific kinetic energy are denoted as p , e , and k respectively. For gas dynamics, $\boldsymbol{\sigma} = -p\mathbf{I}$. The time derivatives are total derivatives that move with the flow. The rate of change of the position is, $\frac{d\mathbf{x}}{dt} = \mathbf{u}$. Please refer to [1] for more details about nomenclatures.

Unknown fields q (e.g., v , \mathbf{u} and τ) can be represented with Taylor expansions on the reference cell Ω about the center of mass.

$$q = \sum_{n=1}^{N(P)} q_n \psi_n \quad (2)$$

where $q_1 = \bar{q}_{cm}$, $q_2 = \left. \frac{\partial q}{\partial \xi} \right|_{cm}$, $q_3 = \left. \frac{\partial q}{\partial \eta} \right|_{cm}$, and $\psi_1 = 1$, $\psi_2 = \xi - \xi_{cm}$, $\psi_3 = \eta - \eta_{cm}$. $N(P)$ means the number of terms for the solution polynomial with degree P ($N(P)$ is equal to 3 for DG(P1)). The subscript cm denotes the center of mass, given by $(\xi_{cm}, \eta_{cm}) = \frac{1}{m} \int_{w(t)} \rho(\xi, \eta) dw$. Here, m denotes the mass of the cell $w(t)$, namely $m = \int_{w(t)} \rho dw$. The basis functions (ψ_n) are constant in time [25]. The evolution equation (e.g., the specific volume equation) is multiplied by the Taylor basis functions and then integrated over the current cell configuration.

$$\int_{w(t)} \psi_m \left(\rho \frac{dv}{dt} - \nabla \cdot \mathbf{u} \right) dw = 0, \quad m = 1, \dots, N(P).$$

Through a set of math operations, the resulting evolution equations for the unknown basis coefficients are,

$$\sum_n M_{mn} \frac{dv_n}{dt} = \oint_{\partial w(t)} \psi_m (\mathbf{n} \cdot \mathbf{u}^*) da - \int_{\Omega} \mathbf{u} \cdot \nabla \psi_m dw, \quad m = 1, \dots, N(P). \quad (3)$$

Here, $M_{mn} = \int_{w(t)} \rho \psi_m \psi_n dw$. The 1st term on the right hand side (rhs) in Eq. (3) requires solving a Riemann problem [12] on the surface of the deformed cell $w(t)$. The Riemann velocity and stress are denoted with a superscript *. The multidirectional approximate Riemann solver for Lagrangian CCH has been explored extensively [9, 10, 12]. The volume integral (the 2nd term on the rhs) is evaluated by Gauss quadrature formulas. An explicit TVD RK method [16] is used to evolve the semi-discrete system of equations.

3. WENO limiting

The Lagrangian DG hydrodynamic method evolves polynomial coefficients forward in time and these polynomial coefficients must be limited near shocks to ensure monotone solutions. In this paper, these solution polynomials are reconstructed using two WENO schemes where the DG solution is the central stencil. It is very important to preserve cylindrical symmetry with WENO on an equal-angle polar mesh for 1D radial flows. To preserve symmetry, two strategies are explored for creating a WENO reconstruction, which are (1) a projection to a local orthonormal basis and (2) a local characteristic decomposition. These strategies are denoted in this paper as strategy 1 and 2.

3.1. Projection to a local orthonormal basis

Step 1. We project the DG solution matrix U in the reference space $(\xi - \eta)$ to the physical space $(x - y)$ for U_p . Here U is the DG solution matrix, defined by,

$$U = \begin{bmatrix} \bar{v} & \frac{\partial v}{\partial \xi} & \frac{\partial v}{\partial \eta} \\ \bar{u} & \frac{\partial u}{\partial \xi} & \frac{\partial u}{\partial \eta} \\ \bar{v} & \frac{\partial v}{\partial \xi} & \frac{\partial v}{\partial \eta} \\ \bar{\tau} & \frac{\partial \tau}{\partial \xi} & \frac{\partial \tau}{\partial \eta} \end{bmatrix}. \quad (4)$$

In the physical space, $q_p = \sum_{n=1}^{N(p)} q_{pn} \phi_n$ with $q_{p1} = \bar{q}_p$, $q_2 = \left. \frac{\partial q_p}{\partial x} \right|_{cm}$, $q_3 = \left. \frac{\partial q_p}{\partial y} \right|_{cm}$ and $\phi_1 = 1$, $\phi_2 = x - x_{cm}$ and $\phi_3 = y - y_{cm}$. Here, (x_{cm}, y_{cm}) is the physical mass center for the cell, namely $(x_{cm}, y_{cm}) = \frac{1}{m} \int_{w(t)} \rho(x, y) dw$. The corresponding polynomial q_p in the physical space can be calculated using L_2 projection,

$$\left[\sum_{n=1}^{N(P)} \int_{w(t)} \rho \phi_m \psi_n dw \right] q_n = \left[\sum_{n=1}^{N(P)} \int_{w(t)} \rho \phi_m \phi_n dw \right] q_{pn}, \quad m = 1, \dots, N(P). \quad (5)$$

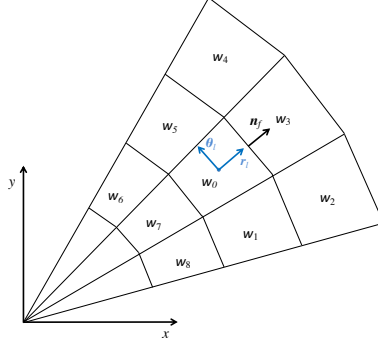


Figure 2: The stencils associated with the cell w_0 . \mathbf{r}_l and $\boldsymbol{\theta}_l$ denote the local orthonormal basis determined by the local cell average velocity. \mathbf{n}_f represents the unit normal vector for the the face f surrounding the cell w_0 .

Likewise, the polynomial matrix in the physical space, U_p , can be obtained.

Step 2. We construct the polynomials q_p^r from the selected stencils. For the cell w_0 , shown in Fig. 2, the following 5 stencils, $\{S_0 : w_0\}$, $\{S_1 : w_0, w_7, w_8, w_1\}$, $\{S_2 : w_0, w_1, w_2, w_3\}$, $\{S_3 : w_0, w_3, w_4, w_5\}$, and $\{S_4 : w_0, w_5, w_6, w_7\}$, have been selected. Here, the polynomial of the central stencil S_0 is known, while the polynomials from other 4 biased stencils need to be reconstructed. For every biased stencil, let's assume the reconstructed polynomial is $q_p^r = \bar{q}_p(w_0) + \frac{\partial q_p^r}{\partial x}(x - x_{cm}(w_0)) + \frac{\partial q_p^r}{\partial y}(y - y_{cm}(w_0))$. Taking stencil S_1 as an example, this polynomial q_p^r satisfies the following,

$$\int \rho q_p^r dw_7 = m(w_7)\bar{q}_p(w_7), \quad \int \rho q_p^r dw_8 = m(w_8)\bar{q}_p(w_8) \quad \text{and} \quad \int \rho q_p^r dw_1 = m(w_1)\bar{q}_p(w_1). \quad (6)$$

Then least squares can be used to calculate q_{p2}^r and q_{p3}^r . Likewise we can get reconstructed polynomial matrix U_p^r for the biased stencils.

Step 3. We compute the smoothness indicator. The smoothness indicator depends on the variable gradient, that is frame dependent and thus leads to rotational symmetry loss.

Step 3.1 Project the polynomial matrix U_p^r to a local orthonormal basis for U_{pl} . For the cell w_0 , we define a local orthonormal basis using the local cell average velocity (u, v) , namely $\mathbf{r}_l = \frac{1}{\sqrt{u^2+v^2}}[u \quad v]^T$ and $\boldsymbol{\theta}_l = \frac{1}{\sqrt{u^2+v^2}}[-v \quad u]^T$, shown in Fig. 2. Therefore, a transformation matrix is introduced,

$$\mathbf{B} = \begin{bmatrix} \frac{\partial r}{\partial x} & \frac{\partial r}{\partial y} \\ \frac{\partial \theta}{\partial x} & \frac{\partial \theta}{\partial y} \end{bmatrix} = \frac{1}{\sqrt{u^2+v^2}} \begin{bmatrix} u & v \\ -v & u \end{bmatrix}. \quad (7)$$

We transform all the stencil polynomials U_p^r in the physical space to the local basis,

$$\begin{cases} \bar{\nu}_{pl} = \bar{\nu}_p^r, & \begin{bmatrix} \bar{u}_{pl} \\ \bar{v}_{pl} \end{bmatrix} = \mathbf{B} \begin{bmatrix} \bar{u}_p^r \\ \bar{v}_p^r \end{bmatrix}, & \begin{cases} \begin{bmatrix} \frac{\partial \nu_{pl}}{\partial r} & \frac{\partial \nu_{pl}}{\partial \theta} \end{bmatrix} = \begin{bmatrix} \frac{\partial \nu_p^r}{\partial x} & \frac{\partial \nu_p^r}{\partial y} \end{bmatrix} \mathbf{B}^{-1} \\ \begin{bmatrix} \frac{\partial \tau_{pl}}{\partial r} & \frac{\partial \tau_{pl}}{\partial \theta} \end{bmatrix} = \begin{bmatrix} \frac{\partial \tau_p^r}{\partial x} & \frac{\partial \tau_p^r}{\partial y} \end{bmatrix} \mathbf{B}^{-1} \end{cases}, & \begin{bmatrix} \frac{\partial u_{pl}}{\partial r} & \frac{\partial u_{pl}}{\partial \theta} \\ \frac{\partial v_{pl}}{\partial r} & \frac{\partial v_{pl}}{\partial \theta} \end{bmatrix} = \mathbf{B} \begin{bmatrix} \frac{\partial u_p^r}{\partial x} & \frac{\partial u_p^r}{\partial y} \\ \frac{\partial v_p^r}{\partial x} & \frac{\partial v_p^r}{\partial y} \end{bmatrix} \mathbf{B}^{-1}. \end{cases} \quad (8)$$

where the subscript l denotes variables in the local basis.

Step 3.2 Calculate the smoothness indicator in context of a local basis. Then the smoothness indicator o_i for a stencil is calculated by,

$$o_i = \max(o_i(\nu_{pl}), o_i(u_{pl}), o_i(v_{pl}), o_i(\tau_{pl})), \quad i = 0, \dots, 4. \quad (9)$$

with $o_i(q_{pl}) = \left(\frac{\partial q_{pl}}{\partial r}\right)^2 + \left(\frac{\partial q_{pl}}{\partial \theta}\right)^2$. Since the terms $\frac{\partial \nu_{pl}}{\partial r}$ and $\frac{\partial \nu_{pl}}{\partial \theta}$ only depend on radius r , the cylindrical symmetry is preserved.

Step 3.3 We compute the nonlinear weights ω_i based on the smoothness indicator o_i ,

$$\omega_i = \frac{\bar{\omega}_i}{\sum \bar{\omega}_i}, \quad \bar{\omega}_i = \frac{\omega l_i}{(\varepsilon + o_i)^2} \quad (10)$$

where ωl_i is a linear weight and $\varepsilon = 10^{-6}$ to avoid division by zero. In this work, $\omega l_0 = 0.5$ and ωl_i for biased stencils is just arithmetic average of $(1 - \omega l_0)$.

Step 3.4. We get the WENO reconstruction polynomial matrix in the local basis using $U_{pl}^w = \sum_{i=0}^4 \omega_i U_{pli}$.

Step 3.5. We project the WENO reconstruction polynomial matrix U_{pl}^w in the local basis back to the physical space for U_p^w using the inverse process of Eq. 8.

Step 4. We Project the WENO-based polynomial matrix U_p^w in the physical space back to the reference space for U using the inverse process of L_2 projection defined in Eq. 5.

3.2. Local characteristic decomposition

Local characteristic decomposition is also applied. Step 1, 2 and 4 are same as that in Section 3.1, while Step 3 is done by a local characteristic decomposition detailed as follows.

Step 3.1 We project the polynomial matrix U_p^r in the physical space to the characteristic field for U_c . The Jacobian matrix of the integral governing equations (Eq. 1) is,

$$\begin{bmatrix} 0 & -n_x & -n_y & 0 \\ -\rho p n_x & -(\gamma - 1)\rho u n_x & -(\gamma - 1)\rho v n_x & (\gamma - 1)\rho n_x \\ -\rho p n_y & -(\gamma - 1)\rho u n_y & -(\gamma - 1)\rho v n_y & (\gamma - 1)\rho n_y \\ -\rho p v_n & -(\gamma - 1)\rho u v_n + p n_x & -(\gamma - 1)\rho v v_n + p n_y & (\gamma - 1)\rho v_n \end{bmatrix}, \quad (11)$$

where $v_n = u n_x + v n_y$. This matrix admits 4 eigenvalues, $\lambda_1 = -\rho c$, $\lambda_2 = \lambda_3 = 0$ and $\lambda_4 = \rho c$. The left and right eigenvectors of such a matrix are,

$$\mathbf{L} = \begin{bmatrix} -\frac{1}{2\gamma} & \frac{n_x}{2\rho c} - \frac{(\gamma-1)u}{2\gamma p} & \frac{n_y}{2\rho c} - \frac{(\gamma-1)v}{2\gamma p} & \frac{\gamma-1}{2\gamma p} \\ \frac{1}{\gamma} & -\frac{n_y v_m}{p} - \frac{u}{p\gamma} & \frac{n_x v_m}{p} - \frac{v}{p\gamma} & \frac{1}{p\gamma} \\ 0 & \frac{n_y}{p} & -\frac{n_x}{p} & 0 \\ \frac{1}{2\gamma} & \frac{n_x}{2\rho c} + \frac{(\gamma-1)u}{2\gamma p} & \frac{n_y}{2\rho c} + \frac{(\gamma-1)v}{2\gamma p} & -\frac{\gamma-1}{2\gamma p} \end{bmatrix} \quad \text{and} \quad \mathbf{R} = \begin{bmatrix} -1 & \gamma - 1 & (\gamma - 1)v_m & 1 \\ \rho c n_x & 0 & p n_y & \rho c n_x \\ \rho c n_y & 0 & -p n_x & \rho c n_y \\ p + \rho c v_n & p & 0 & -p + \rho c v_n \end{bmatrix}. \quad (12)$$

Here, $v_m = v n_x - u n_y$ and c is the sound speed. We project the polynomial matrix U_p^r to the characteristic field,

$$U_{cf} = L_f U_p^r, \quad f = 1, \dots, 4. \quad (13)$$

where the subscript f represent the face number. For L_f (or R_f), n_x and n_y are defined using each normal vector of the 4 faces (Fig. 2) and the variables are obtained using the arithmetic average of averaged variables of the 2 cells sharing the same face.

Step 3.2 We calculate the smoothness indicator based on U_{cf} . Taking the first characteristic variable ν_{cf} as an example,

$$\begin{aligned}\bar{\nu}_{cf} &= -\frac{1}{2\gamma}\bar{\nu} + \left[\frac{n_x}{2\rho c} - \frac{(\gamma-1)u}{2\gamma p}\right]\bar{u} + \left[\frac{n_y}{2\rho c} - \frac{(\gamma-1)v}{2\gamma p}\right]\bar{v} + \frac{\gamma-1}{2\gamma p}\bar{\tau} \\ \frac{\partial \nu_{cf}}{\partial x} &= -\frac{1}{2\gamma}\frac{\partial \nu}{\partial x} + \left[\frac{n_x}{2\rho c} - \frac{(\gamma-1)u}{2\gamma p}\right]\frac{\partial u}{\partial x} + \left[\frac{n_y}{2\rho c} - \frac{(\gamma-1)v}{2\gamma p}\right]\frac{\partial v}{\partial x} + \frac{\gamma-1}{2\gamma p}\frac{\partial \tau}{\partial x} \\ \frac{\partial \nu_{cf}}{\partial y} &= -\frac{1}{2\gamma}\frac{\partial \nu}{\partial y} + \left[\frac{n_x}{2\rho c} - \frac{(\gamma-1)u}{2\gamma p}\right]\frac{\partial u}{\partial y} + \left[\frac{n_y}{2\rho c} - \frac{(\gamma-1)v}{2\gamma p}\right]\frac{\partial v}{\partial y} + \frac{\gamma-1}{2\gamma p}\frac{\partial \tau}{\partial y}\end{aligned}\quad (14)$$

For sake of brevity, the superscript r and subscript p are omitted. Combining with Eq. 7,

$$\begin{aligned}\left(\frac{\partial \nu_{cf}}{\partial x}\right)^2 + \left(\frac{\partial \nu_{cf}}{\partial y}\right)^2 &= \left(d_1\frac{\partial \nu}{\partial x} + d_2\frac{\partial u_{pl}}{\partial x} + d_3\frac{\partial \tau}{\partial x}\right)^2 + \left(d_1\frac{\partial \nu}{\partial y} + d_2\frac{\partial u_{pl}}{\partial y} + d_3\frac{\partial \tau}{\partial y}\right)^2 \\ &= \left(d_1\frac{\partial \nu}{\partial r} + d_2\frac{\partial u_{pl}}{\partial r} + d_3\frac{\partial \tau}{\partial r}\right)^2 + \left(d_1\frac{\partial \nu}{\partial \theta} + d_2\frac{\partial u_{pl}}{\partial \theta} + d_3\frac{\partial \tau}{\partial \theta}\right)^2\end{aligned}\quad (15)$$

with $d_1 = -\frac{1}{2\gamma}$, $d_2 = \frac{1}{2\rho c} - \frac{(\gamma-1)\sqrt{2k}}{2\gamma p}$, $d_3 = \frac{\gamma-1}{2\gamma p}$ and $u_{pl} = un_x + vn_y$. It can be observed that $\left(\frac{\partial \nu_{cf}}{\partial x}\right)^2 + \left(\frac{\partial \nu_{cf}}{\partial y}\right)^2$ only depend on the radius, thus it preserves the cylindrical symmetry. Step 3.3 and 3.4 are similar to the above section. The above 4 steps are executed four times (4 faces) for creating the WENO reconstruction.

Step 3.5 We transform the 4 reconstructed polynomial U_{cf}^w in the characteristic field back to the physical space for U_{pf}^w using the inverse process of Eq. 13, namely,

$$U_{pf}^w = R_f U_{cf}^w, \quad f = 1, \dots, 4. \quad (16)$$

Step 3.6 The final sole polynomial U_p^w for the physical space is just the arithmetic average of the 4 polynomials U_{pf}^w .

4. Test problems

In this section, a suite of challenging test problems are calculated to demonstrate the accuracy and robustness of the WENO-based Lagrangian DG hydrodynamic method. The test problems are the polar Sod [20], Sedov [35] and Noh [36], which all use a gamma-law equation of state (EOS). Some important parameters are listed in Table 1. The initial conditions (ρ^0, u^0, v^0, p^0) for polar Sod (left), Sedov (middle) and Noh (right) are given by,

$$\left\{ \begin{array}{l} (1, 0, 0, 1), \\ (0.125, 0, 0, 0.1), \end{array} \right. \quad r < 0.5 \quad \left\{ \begin{array}{l} (1.0, 0, 0, (\gamma-1)\frac{\rho_o E_o}{w_o}), \\ (1.0, 0, 0, 10^{-6}), \end{array} \right. \quad \begin{array}{l} \text{Origin} \\ \text{Others} \end{array}, \quad \left\{ \begin{array}{l} (1.0, \frac{-x}{\sqrt{x^2+y^2}}, \frac{-y}{\sqrt{x^2+y^2}}, 10^{-6}), \\ \end{array} \right.$$

where $r = \sqrt{x^2 + y^2}$ for the polar Sod problem. With the Sedov problem, 'Origin' means the cells containing the origin and w_o denotes the cell volume and $E_o = 0.244816$.

Table 1: Important parameters for different cases

	Gas constant (γ)	Computational domain	Mesh resolution	Final time
Sod shock tube	1.4	$[0.01, 1] \times [0, 2\pi]$	99×48	0.2
Sedov blast	1.4	$[-1.2, 1.2] \times [-1.2, 1.2]$	60×60	1.0
Noh implosion	5/3	$[-1.0, 1.0] \times [-1.0, 1.0]$	100×100	0.6

The numerical results are shown in Fig. 3. For all test cases, the meshes in the first quadrant are presented. The final meshes (Fig. 3a, 3d and 3g) move in a stable manner. The density scatter plots (Fig. 3b, 3e and 3h) agree well with the exact solution. The polar Sod problem is used to do the quantitative analysis of symmetry preserving. Velocity deviations from the radial direction are used as a symmetry-preserving metric. From the scatter plots for symmetry errors shown in Fig. 3c, our two strategies preserve symmetry very well as demonstrated by the fact that the largest errors are on the order of 10^{-15} (machine precision), while the original WENO method cannot preserve symmetry. From Fig. 3f, for Sedov, strategy 2 gives the smallest density scatter as expected. In addition, the difference between the original WENO method and strategy 1 is very small because the original method happens to preserve symmetry on an initially uniform square mesh for this kind of symmetric explosion problem; the explanation is as follows. Taking the first quadrant as an example, the test problem and the mesh are both symmetric about the 45° line so the smoothness indicators for the two symmetric cells about the 45° line are equal. Likewise, a similar phenomenon can be observed for the Noh problem.

5. Conclusions

We presented new symmetry-preserving WENO limiters and used them with a Lagrangian DG hydrodynamic method to simulate shock driven flows in 2D Cartesian coordinates. The WENO reconstructions were calculated using two approaches (1) a projection to a local orthonormal basis or (2) using a local characteristic decomposition to preserve cylindrical symmetry on an equal-angle polar mesh for radial flows. The DG solution is used as the central stencil for the WENO reconstructions in this work; however, these WENO schemes could also be used with finite volume hydrodynamic methods where the central stencil is constructed by least squares fitting neighboring cell average values. The symmetry preservation of the new WENO schemes with the Lagrangian DG hydrodynamic method was demonstrated by calculating the polar Sod problem. The canonical WENO method breaks symmetry, while the new WENO schemes have errors on the order of machine precision. The accuracy and robustness of the proposed WENO schemes was then demonstrated by calculating the Sedov and Noh test problems. These new WENO schemes are a promising approach for calculating limited reconstructions for use with finite volume and DG hydrodynamic methods.

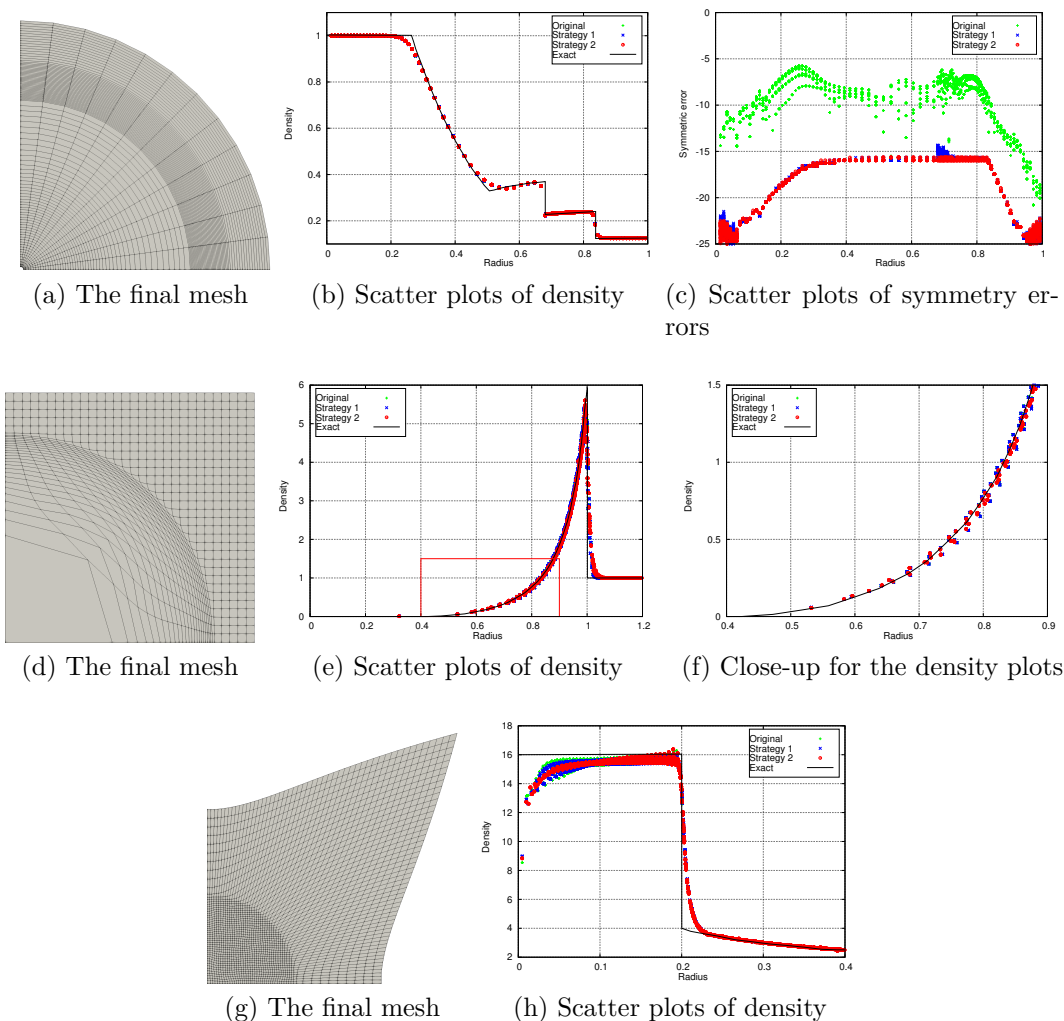


Figure 3: The numerical results are shown for different cases. The 1st, 2nd, and 3rd row show the numerical results for the Sod shock tube, Sedov blast wave and Noh implosion test problems respectively.

6. Acknowledgments

We gratefully acknowledge the support of the NNSA through the Laboratory Directed Research and Development (LDRD) program at Los Alamos National Laboratory. The Los Alamos unlimited release number is LA-UR-19-22578.

References

- [1] X. Liu, N. Morgan, and D. Burton. A Lagrangian discontinuous Galerkin hydrodynamic method. *Computers & Fluids*, 163:68–85, 2018.
- [2] J von Neumann and R Richtmyer. A method for the calculation of hydrodynamics shocks. *Journal of Applied Physics*, 21:232–237, 1950.
- [3] M. Wilkins. Use of artificial viscosity in multidimensional shock wave problems. *Journal of Computational Physics*, 36:281–303, 1980.

- [4] D. Burton. Multidimensional discretization of conservation laws for unstructured polyhedral grids. Technical Report UCRL-JC-118306, Lawrence Livermore National Laboratory, 1994.
- [5] E. Caramana, D. Burton, M. Shashkov, and P. Whalen. The construction of compatible hydrodynamic algorithms utilizing conservation of total energy. *Journal of Applied Physics*, 146:227–262, 1998.
- [6] N. Morgan, K. Lipnikov, D. Burton, and M. Kenamond. A Lagrangian staggered grid Godunov-like approach for hydrodynamics. *Journal of Computational Physics*, 259:568–597, 2014.
- [7] S.K. Godunov, A. Zabrodine, M. Ivanov, A. Kraiko, and G. Prokopov. Résolution numérique des problèmes multidimensionnels de la dynamique des gaz. *Mir*, 1979.
- [8] S. Godunov. Reminiscences about difference schemes. *Journal of Computational Physics*, 153:6–25, 1999.
- [9] B. Després and C. Mazeran. Lagrangian gas dynamics in two dimensions and Lagrangian systems. *Arch. Rational Mech. Anal.*, 178:327–372, 2005.
- [10] P-H. Maire, R. Abgrall, J. Breil, and J. Ovadia. A cell-centered Lagrangian scheme for two-dimensional compressible flow problems. *SIAM Journal Scientific Computing*, 29:1781–1824, 2007.
- [11] P-H. Maire. A high-order cell-centered Lagrangian scheme for two-dimensional compressible fluid flows on unstructured mesh. *Journal Computational Physics*, 228:2391–2425, 2009.
- [12] D. Burton, T. Carney, N. Morgan, S. Sambasivan, and M. Shashkov. A cell centered Lagrangian Godunov-like method of solid dynamics. *Computers & Fluids*, 83:33–47, 2013.
- [13] W. Boscheri and M. Dumbser. A direct Arbitrary-Lagrangian-Eulerian ADER-WENO finite volume scheme on unstructured tetrahedral meshes for conservative and non-conservative hyperbolic systems in 3D. *Journal of Computational Physics*, 275:484–523, 2014.
- [14] N. Morgan, M. Kenamond, D. Burton, T. Carney, and D. Ingraham. An approach for treating contact surfaces in Lagrangian cell-centered hydrodynamics. *Journal of Computational Physics*, 250:527–554, 2013.
- [15] B. Cockburn, S. Hou, and C.-W. Shu. The Runge-Kutta local projection discontinuous Galerkin finite element method for conservation laws. IV. The multidimensional case. *Mathematics of Computation*, 54:545–581, 1990.
- [16] B. Cockburn and C.-W. Shu. The Runge-Kutta discontinuous Galerkin method for conservation laws V: multidimensional systems. *Journal of Computational Physics*, 141:199–224, 1998.
- [17] H. Luo, J. Baum, and R. Löhner. A discontinuous Galerkin method based on a Taylor basis for the compressible flows on arbitrary grids. *Journal of Computational Physics*, 227:8875–8893, 2008.
- [18] X. Liu, L. Xuan, Y. Xia, and H. Luo. A reconstructed discontinuous Galerkin method for the compressible Navier-Stokes equations on three-dimensional hybrid grids. *Computers & Fluids*, 152:271–230, 2017.
- [19] Z. Jia and S. Zhang. A new high-order discontinuous Galerkin spectral finite element method for Lagrangian gas dynamics in two-dimensions. *Journal of Computational Physics*, 230:2496–2522, 2011.
- [20] F. Vilar. Cell-centered discontinuous Galerkin discretization for two-dimensional Lagrangian hydrodynamics. *Computers & Fluids*, 64:64–73, 2012.
- [21] F. Vilar, P-H. Maire, and R. Abgrall. A discontinuous Galerkin discretization for solving the two-dimensional gas dynamics equations written under total Lagrangian formulation on general unstructured grids. *Journal of Computational Physics*, 276:188–234, 2014.
- [22] E. Lieberman, N. Morgan, D. Luscher, and D. Burton. A higher-order Lagrangian discontinuous Galerkin hydrodynamic method for elastic-plastic flows. *submitted to Computers & Fluids*.
- [23] X. Liu, N. Morgan, and D. Burton. Lagrangian discontinuous Galerkin hydrodynamic methods in axisymmetric coordinates. *Journal of Computational Physics*, 373:253–283, 2018.
- [24] N. Morgan, X. Liu, and D. Burton. Reducing spurious mesh motion in Lagrangian finite volume and discontinuous Galerkin hydrodynamic methods. *Journal of Computational Physics*, 372:35–61, 2018.
- [25] X. Liu, N. Morgan, and D. Burton. A high-order Lagrangian discontinuous Galerkin hydrodynamic method for quadratic cells using a subcell mesh stabilization scheme. *Journal of Computational Physics*, 386:110–157, 2019.
- [26] T. Barth and D.C. Jespersen. The design and application of upwind schemes on unstructured meshes.

- 27th Aerospace Sciences Meeting, AIAA 1989-366, Reno, NV, 1989.
- [27] D. Kuzmin. A vertex-based hierarchical slope limiter for p-adaptive discontinuous Galerkin methods. *Journal of Computational and Applied Mathematics*, 233(12):3077–3085, 2010.
 - [28] R. Abgrall. On essential non-oscillatory schemes on unstructured meshes. *Journal of Computational Physics*, 114:45–58, 1994.
 - [29] G-S Jiang and C.-W. Shu. Efficient implementation of weighted ENO schemes. *Journal of Computational Physics*, 126:202–228, 1996.
 - [30] H. Luo, J. Baum, and R. Löhner. A Hermite WENO-based limiter for discontinuous Galerkin method on unstructured grids. *Journal of Computational Physics*, 225:686–713, 2007.
 - [31] J. Qiu and C.-W. Shu. Hermite WENO schemes and their application as limiters for Runge-Kutta discontinuous Galerkin method: one-dimensional case. *Journal of Computational Physics*, 193:115–135, 2004.
 - [32] J. Cheng and C.-W. Shu. A cell-centered Lagrangian scheme with the preservation of symmetry and conservation properties for compressible fluid flows in two-dimensional cylindrical geometry. *Journal of Computational Physics*, 229:7091–7206, 2010.
 - [33] P-H. Maire, R. Loubère, and P. Vachal. Staggered Lagrangian discretization based on cell-centered Riemann solver and associated hydrodynamics scheme. *Communications in Computational Physics*, 10:940–978, 2011.
 - [34] C.-W. Shu. Essentially non-oscillatory and weighted essentially non-oscillatory schemes for hyperbolic conservation laws, in: B. Cockburn, C. Johnson, C.-W. Shu, E. Tadmor, A. Quarteroni (Eds.), *Advanced Numerical Approximation of Nonlinear Hyperbolic Equations*, Lecture Notes in Math. 1697. pages 325–432, 1998.
 - [35] L. Sedov. *Similarity and dimensional methods in mechanics*, 1959.
 - [36] W. Noh. Errors for calculations of strong shocks using an artificial viscosity and an artificial heat flux. *Journal of Applied Physics*, 72:78–120, 1987.